S. Afr. J. Chem., 2026, 80, S129–S140
https://journals.co.za/content/journal/chem/

1,4,7-Triazacyclononane-1,4,7-Triacetic Acid Exhibits Potent Inhibition Against HIV-1 IN Subtype B and South African Subtype C (C-SA)

Nakita Reddy[1,2], Kevyna Chetty[1], Sibusiso Maseko[1,3], Darian Naidu[4], Charmaine Kahiya[1], Glenn E. M. Maguire[1,5], Tricia Naicker[1], Thavendran Govender[6], Johnson Lin[7], Nompumelelo P. Mkhwanazi[4] and Hendrik G. Kruger[1]*

[1]*Catalysis and Peptide Research Unit, University of KwaZulu-Natal, Durban, South Africa.*
[2]*Office of AIDS and TB, South African Medical Research Council, Pretoria, South Africa.*
[3]*GIGA-Molecular Biology of Diseases, Protein Signalling and Interactions, University of Liege, Liege, Belgium.*
[4]*HIV Pathogenesis Programme, School of Medicine, University of KwaZulu-Natal, Durban, South Africa.*
[5]*Discipline of Chemistry, University of KwaZulu-Natal, Durban, South Africa.*
[6]*Department of Chemistry, University of Zululand, KwaDlangezwa, South Africa.*
[7]*School of Life Sciences, University of KwaZulu-Natal, Durban, South Africa.*

ABSTRACT

Human immunodeficiency virus (HIV) drug resistance has compromised antiretroviral therapy (ART) efficacy, highlighting the need for new treatment options. This study evaluates the macrocyclic chelator 1,4,7-triazacyclononane-1,4,7-triacetic acid (NOTA) as a potential anti-HIV agent targeting the zinc ions in the N-terminal domain of HIV-1 integrase (IN). Recombinant techniques were used to produce IN subtypes B and C-SA, and NOTA's activity was assessed through enzymatic and thermodynamic assays. Despite not reaching statistical significance ($p = 0.061$), NOTA displayed potent inhibition, with K_{iapp} values of 6.8 ± 0.03 nM and 8.0 ± 0.15 nM against subtypes B and C-SA, respectively, suggesting enhanced inhibitory potential compared with the commercial INSTIs dolutegravir and raltegravir. Notably, NOTA demonstrated greater potency and a higher Gibbs free energy (-9.8 kcal/mol) against subtype B, as compared to commercial INSTIs. The antiviral studies demonstrated that NOTA inhibits both HIV-1 subtype B and subtype C, with particularly high inhibitory activity against subtype C. Mechanistic investigations indicate that NOTA blocks HIV integration, likely by interfering with either the strand transfer process or nuclear import. Molecular docking of HIV-1 subtype B and subtype C(SA) in AutoDock Vina provided structural validation, with no significant difference between the two subtypes (ΔG: -5.98 vs -6.00 kcal/mol, p = 0.347). These results indicate favourable binding energies for zinc chelation. This study suggests NOTA and other zinc chelators could offer a new mechanism for inhibiting HIV-1 integrase and serve as promising candidates for HIV therapy.

KEYWORDS

HIV-1 Integrase, Subtype B, South African Subtype C, Integrase Strand Transfer Inhibitors, macrocyclic chelator NOTA

Received: 16 February 2026 Revised: 10 April 2026 Accepted: 11 May 2026

INTRODUCTION

Globally, approximately 40.8 million people are living with Human immunodeficiency virus (HIV) and Acquired Immunodeficiency Syndrome (AIDS),[1, 2] through antiretroviral therapy (ART), which has improved life expectancy. However, extensive use of ARTs has led to the development of resistance-associated mutations and the transmission of drug resistance.[3, 4] HIV is a retrovirus that requires integration of its genome into the host cell for replication, and this process is catalysed by the retroviral integrase (IN).[2] HIV type 1 (HIV-1) IN has emerged as a clinically validated antiretroviral drug target for the treatment of HIV due to its high therapeutic index and specificity for the integration process. [5] IN is a 32 kDa protein with 288 amino acid residues encoded by the 3' end of the HIV-1 *pol* gene.[6] It also consists of three distinct structural domains: a catalytic core, an N-terminal and a C-terminal.[7]

The first integration phase occurs when the dinucleotide from each 3'end of viral DNA is cleaved, also known as the 3'end processing. This reaction also requires a conserved nucleotide sequence, positioned at the viral DNA ends.[8] Subsequently, DNA strand transfer occurs when the 3'-processed DNA ends of the same viral DNA are inserted into the host's cellular DNA.[9] The N-terminal domain adopts two CCHC zinc finger motifs that are vital for the replication of the retroviruses.[10] The zinc finger motif contains highly conserved histidine (His) and cysteine (Cys) residues. Zinc ions bind to these motifs to stabilise the domain folded state of IN, whilst enhancing enzymatic activity.[11, 12]

Research focused on utilizing HIV-1 IN as drug targets has led to significant advancements in the treatment of HIV with the approval of IN strand transfer inhibitors (INSTIs); raltegravir (RAL; MK-0518),[13] elvitegravir (EVG; GS-9137),[14] dolutegravir (DTG; S/GSK1349572),[15] and bictegravir (BIC)[16] and more recently, cabotegravir (CAB)[17, 18] by the Food and Drug Administration (FDA). Their mechanism of action involves inhibiting the HIV-1 IN strand transfer reaction to prevent the integration of the viral DNA into the host cell's chromosomal DNA. This occurs when the drugs selectively bind the cleaved stable synaptic complex and interfere with the formation of the strand transfer complex.[19, 20]

Non-catalytic site IN inhibitors (NCINIs), however, inhibit the allosteric pocket of the enzyme and hinders the integration of IN with viral DNA and essential cellular co-factors such as lens epithelium-derived growth factor/ protein 75 (LEDGF/p75).[21, 22] Nevertheless, the emergence of resistance mutations with INSTIs and a lack of FDA-approved NCINIs emphasizes the need for the development of IN inhibitors with a different mechanism of action.

Zinc chelation offers one solution for IN inhibition, and has been examined previously, as observations from *N*,*N*,*N*,*N*-tetrakis(2-pyridylmethyl)ethylenediamine (TPEN) show HIV-1 Vif protein inhibition as well as degradation of HIV-1 via the APOBEC3G enzyme.[10] Another report by Pannecouque et al.,[10] highlights *N*,*N*-bis(4-ethoxycarbonyl-1,2,3-thiadiazol-5-yl)benzene-1,2-diamine as

*To whom correspondence should be addressed
Email: kruger@ukzn.ac.za

ISSN 1996-840X Online / South African Chemical Institute / http://saci.co.za/journal
© The Author(s) Published under a Creative Commons Attribution 4.0 International Licence (CC BY 4.0)
https://doi.org/10.17159/0379-4350/2026/v80se1a14

a chelator of the zinc fingers (zinc ejector) present on nucleocapsid protein 7 (NCp7). Other zinc ejectors that have been reported[23] include: 3-nitrosobenzamide (NOBA)[24] from the C-nitroso-class, 2,2-dithiobisbenzamide disulfides (DIBA),[25] pyridinioalkanoyl thioesters (PATE),[26] and Sacyl- 2 mercaptobenzamide thioesters (SAMT).[27] Currently, two zinc injectors are undergoing clinical trials: azodicarbonamide (ADA) in Europe, and benzisothiazolone (BITA), derived from DIBA-4, in the United States.[28]

The macrocyclic chelator: 1,4,7-triazacyclononane-1,4,7-triacetic acid (NOTA) is a non-toxic bi-functional chelating agent,[29] often utilized for radiotherapy and radio-imaging and can complex metal ions with high thermodynamic stability. NOTA and its derivatives were shown to exhibit excellent bactericidal activity against carbapenem-resistant Enterobacteriaceae by chelating zinc ions from the metallo-β-lactamase active site, thus neutralizing the enzyme and potentiating the activity of meropenem.[30, 31] In these studies, this agent exhibited specific activity toward the zinc ions present at the metallo β-lactamase active site. There were no observations of off-target specificity towards zinc-containing metallo-enzyme, Glyoxylase-II.[31] The exact mechanism of binding in these systems is unclear, but it does appear to be irreversible,[31] and further studies are required. However, this does not detract from its development as a clinical inhibitor. As NOTA has the potential to safely and effectively bind to the zinc ions of the active site of the N-terminal domain of IN, it appears to have potential as an HIV-1 IN inhibitor. Therefore, a hypothesis was initiated, of utilizing this compound as a new class of NCINI for HIV-1.[32]

HIV-1 IN subtype B has been the central focus for antiretroviral drug design, whilst most patients in Southern Africa are largely infected with subtype C.[33, 34] Although IN inhibitors have been active against both subtypes in therapy,[35] only a few reports on the effectiveness of commercially available HIV-1 IN drugs exist on the South African subtype C (subtype C-SA). The purpose of this study was to determine the enzyme activities and experimental binding energies of commercial INSTIs and NOTA between HIV-1 subtype B and subtype C-SA IN enzymes. In addition, it aims to assess whether NOTA could function as a potential inhibitor of HIV-1 IN.

METHODS

The NOTA was obtained from DLD Scientific, South Africa, and used without further purification.

HIV-1 Integrase Subtypes and Materials

Plasmids containing the HIV-1 IN subtype B and C-SA gene, respectively, were purchased from GenScript USA Inc. according to the HIV-1 IN sequences. The 38-mer oligonucleotide substrate used[36] as the IN substrate was synthesised from Inqaba Biotech (South Africa). INSTIs; Dolutegravir and Raltegravir were purchased from Leap Labchem (China). NOTA, cobalt chromatography cartridges and the chemical reagents utilized were purchased from Thermo-Fisher Scientific (USA) unless stated otherwise.

Verification of HIV-1 Integrase

Competent *E. coli* BL21 (DE3) cells (obtained from the Microbiology Department at the University of KwaZulu-Natal) were transformed with the recombinant plasmid (pET320-His) and grown overnight on Luria-Bertani (LB) (10 g/L of tryptone, 5 g/L of yeast extract and 5 g/L NaCl) plates containing ampicillin (100 µg/ml). Positive clones of both subtype B and C-SA were screened and verified by restriction digestion as well as colony PCR with primers containing EcoRI and XhoI restriction sites in the forward and reverse primers respectively; subtype B (Forward: 5'-GAA TTC TTT TTA GAT GGA ATA GAT AAG GCC-3' and reverse: 5'-CTC GAG TTA ATC CTC ATC CTG TCT-3') as well as subtype C-SA (Forward: 5'-GAA TTC CTA ATC CTC ATC CTG TCT ACC TGC-3' and reverse: 5'-CTC GAG TTT TTA GAT GGG ATA GAT-3'). The coding sequence of both subtypes was mutated to introduce the amino acid substitutions F185K and C280S to increase IN solubility. In addition, the N-terminal is in frame with the poly (His)6-tag. The PCR fragments of Subtype B and C-SA were analysed using a 1.2% (w/v) agarose gel. The gel was visualized by staining with 0.5 µg/ml ethidium bromide. Electrophoresis conditions included a run at 100 V, 64 mA for approximately 40 min.[37] The gel image was captured using the Syngene Gel documentation system (Vacutec South Africa).

Expression of HIV-1 Integrase

Ampicillin-containing LB broth was inoculated with 1 mL of the overnight cultures at 37°C, with agitation of 200 rpm until the cells reached an OD 600 nm of 0.5. Thereafter, cells were induced with one mM Isopropyl β-D-1-thiogalactopyranoside (IPTG). Three hours post-induction, the cells were harvested and centrifuged at 10,000 *x g* for 5 min at 4°C. Pellets were resuspended in 25 mL of 50 mM Tris-HCl (pH 7.7). Sonication (Omni International Sonic Ruptor 400 Ultrasonic homogenizer) was used to disrupt the cells at an operating frequency of 60 kHz for 10 min. Thereafter, samples were centrifuged for 15 min at 4°C and 10,000 *x g*.[38]

Purification of HIV-1 Integrase

Crude proteins were purified using a 5 mL cobalt affinity column. The column was pre-equilibrated with two column volumes (CVs) of equilibration/wash buffer (20 mM sodium phosphate, 300 mM NaCl, and 5 mM imidazole). Crude proteins (25 mL) were loaded onto the column and washed with five CVs of the same buffer. A portion of the flow-through was collected, and bound proteins were eluted using elution buffer (20 mM sodium phosphate, 300 mM NaCl, and 300 mM imidazole).[39, 40] The purity of the protein fractions for each subtype was confirmed by sodium dodecyl sulfate-polyacrylamide gel electrophoresis (SDS-PAGE). The concentration of the fractions that contained purified proteins was determined by using the Nanodrop 2000 UV-Vis Spectrophotometer. The extinction coefficient used for subtype B was 50 795 M-1cm-1 and 53 775 M-1cm-1 for subtype C-SA, calculated using analysis tools on the Expasy server.[41] Fractions containing purified protein were pooled together per subtype and dialysed against the buffer (25 mM HEPES (pH 7.0), 10 mM β-mercaptoethanol, 5% glycerol, 0.1 g/L BSA, and 10 mM MnCl2) overnight at 4°C.

Sodium Dodecyl Sulfate–Polyacrylamide Gel Electrophoresis (SDS-PAGE)

The analysis of the crude extract, supernatant, and purified HIV-1 proteins was carried out by SDS-PAGE analysis[42] with a 15% acrylamide gel. The acrylamide gel was stained overnight using Coomassie brilliant blue R250 (0.05%) and de-stained with a solution [40% (v/v) methanol and 10% acetic acid (v/v)]. The image of SDS-PAGE was captured using the Syngene Gel documentation system (BioGenie System 2).

HIV-1 integrase 3' Processing Activity Assay

A 3'-processing kinetic assay was performed to evaluate the enzymatic activity of HIV-1 IN subtype B and C-SA as described by Hong-qui *et al.*[36] The assay was performed at 37°C in 96-well plates that had a final volume of 100 µL in each well containing the reaction buffer (25 mM HEPES (pH 7.0), 10 mM β-mercaptoethanol, 5% glycerol, 0.1 g/L BSA and 10 mM MnCl2 and 65 nM purified HIV-1 IN of subtype B and C-SA, respectively. The reaction was then initiated by the addition of the 38-mer oligonucleotide substrate (5'-[FAM]-ACT GCT AGA GAT TTT CCA CGT GGA AAA TCT CTA GCA GT-[BHQ-1]-3'), which varied in concentration (0 - 400 nM). Notably, the sequence is identical to the unique 5' (U5) region of the viral long terminal repeats

(LTR) and results in a stem-loop structure with the fluorophore at the 5' end and a quencher at the 3'end. Moreover, HIV-1 IN is specific and sensitive to the oligonucleotide substrate, thus IN cleaves the terminal 3' dinucleotide, which contains the quencher, increasing fluorescence.[36] A 34-mer control, which has the first two (AC) and last two nucleotides (GT) of the assay substrate, has been removed. A negative control was used, and measurements were evaluated based on the negative control. A fluorescence signal was detected and monitored using the Jasco V-630 spectrofluorometer (Jasco International Co., Ltd, Japan). The instrument was set to read fluorescence signals at 485 nm excitation and 535 nm emission. Kinetic curves were prepared for subtype B and C-SA as described by He *et al.*[36] so that activity plots in the linear range could be constructed and analysed. The data obtained was then analysed using GraphPad Prism, version 5.01 (GraphPad Software, Inc.) to determine kinetic parameters.[9]

Inhibition Studies

Inhibition studies were carried out to inhibit the IN 3'-processing activity.[43] Apparent inhibition constants (K_{iapp}) for the selected FDA-approved INSTIs (Dolutegravir and Raltegravir) and a chelating agent (NOTA) were evaluated for both subtypes at 37°C in 96-well plates as described above, but varying 38-mer oligonucleotide substrate (0-20 nM) in the presence of increasing concentrations of the inhibitor (0-10 nM). The competitive inhibition equation was used to calculate the K_{iapp} values.[31]

Thermodynamic Measurement using Fluorescence Quenching

Spectroscopic methods, specifically fluorescence spectroscopy, provide details about ligand-protein binding, which includes the strength, type, and mechanism of the binding.[44] Hence, a tertiary structural alteration that is induced in HIV-1 IN by the inhibitors can be determined by observing the interaction that occurs between each drug and the purified enzymes. The reaction was monitored with the Jasco V-630 spectrofluorometer (Jasco International Co., Ltd, Japan). As tryptophan residues serve as a local probe in their immediate environment in the HIV-IN protein, they were selectively excited at 295 nm, whilst the emission wavelength was set at 482 nm. The change in fluorescence was monitored over 10 min at 1 min incubation intervals as increasing concentrations of INSTIs (2 nM, 5 nM, 10 nM) were added to the reaction mixture containing 65 nM HIV-1 IN in the reaction buffer that made up a final volume of 100 µL. All fluorescence quenching experiments were carried out at three different temperatures (293 K, 298 K, 303 K). Calculations of the thermodynamic parameters were derived from the Stern-Volmer and Van't Hoff graphical plots[40, 45, 46] using the appropriate equations (Supplementary information).

Biological assay: Cell lines and culture conditions

TZM-bl cells are a genetically modified HeLa clone that expresses CD4 and CCR5 receptors. These receptors predispose the cells to HIV-1 infection.[47] TZM-bl cells have an integrated firefly luciferase reporter gene that is controlled by the HIV-1 long terminal repeat (LTR) promoter, allowing infection levels to be quantified using luminescence.[48] The 293 T cells were used to produce the HIV-1 virus. For the experiments, TZM-bl cells and 293 T cell lines (derived from human embryonic kidney (HEK293)) were cultured in Dulbecco's Modified Eagle Medium (DMEM) (Thermo Fisher Scientific, Waltham, United States of America) supplemented with 10% fetal bovine serum (FBS) (LTC Biosciences, Gainesville, United States of America) and 1% penicillin-streptomycin. The cells were incubated at 37°C in an incubator containing 5% CO_2. The cells were rinsed with phosphate-buffered saline (PBS) (Thermo Fisher Scientific, Waltham, United States of America) before being treated with a 37 °C pre-heated trypsin-EDTA solution. Following separation, trypsin was completely neutralized with growth media before the cells were gently resuspended. Passaging was done every 2-3 days. Before the cells' were passaged, their vitality was determined by staining with trypan blue, followed by cell counts. The trypan blue staining principle works on the concept that viable cells have intact cell membranes that keep the dye out, whereas non-viable cells do not have intact membranes and therefore stain blue.

MTT (3-[4,5dimethylthiazol-2-yl]-2,5 diphenyl tetrazolium bromide) assay to assess the cytotoxicity of NOTA

The cell cytotoxicity and viability of NOTA were tested on TZM-bl cell lines using the MTT method described by Naidu et al (2025).[49] Briefly, to a 96-well microplate, 100 µL of DMEM was added to the first column, representing the media control. The second column represented the cell control and contained 150 µL of DMEM and 140 µL of the sample. Azidothymidine (AZT) served as the positive drug control. The test sample in a volume of 10 µL was then added. Serial dilutions in the volume of 50 µL were then performed, followed by the addition of 100 µL of the prepared cell suspension (10,000 TZM bl cells). The plate was then incubated for 48 hours at 37°C in a 5% CO_2 environment. After incubation, 10 µl of the MTT (5mg/ml MTT salt in PBS) solution was applied to each well except the control wells. The plate was then incubated for a further 4 hours at 37 °C with 5% CO_2. Thereafter, 75 µL of sample medium was removed from the experimental and positive control wells and added to 50 µL of dimethyl sulfoxide (DMSO) to dissolve the formazan crystals. Using a Perkin Elmer microplate reader, the absorbance was recorded at a wavelength of 450 nm. The concentration resulting in 50% cytotoxicity (CC_{50}) was calculated using GraphPad Prism version 5.01 by generating a dose-response curve (concentration versus sample cell viability percentage).

% Cell viability = [(sample absorbance − mean media control absorbance − free sample blank) / (cell absorbance)] × 100

Anti-HIV-1 activity screening of NOTA using the Luciferase-based assay

A luciferase-based assay was used to evaluate the anti-HIV-1 activity of the NOTA as explained by Sarzotti-Kelsoe et al.,[48] and Kubheka et al.[50] In brief, to a 96-well microplate, 100 µL of DMEM was added to the first column representing the cell control, 150 µL was added to the second column, representing the virus control and 140 µL was added to the remaining columns as the drug and sample controls. To the drug control and samples columns, 11 µL of 1000 µg/mL of Raltegravir, Dolutegravir, Elvitagravir and NOTA, respectively, was added and serially diluted. TZM-bl cells were cultured for one hour at 37°C with 5% CO_2. Then 50 µL of HIV-1 subtype B NL4.3 and subtype C SK388 virus, respectively, were added at the 50% Tissue Culture Infectious Dose (TCID50) dose, except for the cell control. The 96-well microplate was then incubated for one hour at 37°C with 5% CO_2. Then, 100 µL of 10,000 TZM-bl cells in DMEM with 44 µg/mL DEAE-dextran was added to all wells. The 96-well microplate was then incubated for 48 hours at 37°C with 5% CO_2. Following incubation, 100 µL of Bright-Glo luciferase reagent was added to each well in place of 150 µL of culture media. To ensure full cell lysis, the plates were incubated for two minutes at room temperature in the dark. Following the transfer of 150 µL of the lysate to a corresponding 96-well black plate, luminescence was promptly measured at 540 nm using a Victor Nivo multimode plate reader (PerkinElmer, US). The percentage inhibition was calculated as the difference in the average relative luminescence units (RLUs) of the virus control wells divided by the difference between the RLUs of the test wells (cells + drug + virus) and the cell control wells (cells only). The GraphPad Prism software (v.5.00.288) was used to determine the half-maximal inhibitory concentration (IC_{50}). Data analysis was done using the average of the three assay repetitions.

Time of addition assay

The anti-HIV drug's interactions with the HIV-1 replication cycle were ascertained using the time of addition assay according to Kubheka et al.[50] Briefly, a 96-well cell culture microplate was seeded with 150 µL of 10,000 TZM-bl cells and incubated at 37 °C with 5% CO_2. Thereafter, 50 µL of each of the HIV-1 subtypes B and C viruses pNL4.3 and SK388 were added, followed by 15 µL of antiretroviral controls azidothymidine (at 5 hours), raltegravir, dolutegravir and elvitegravir (at 8 and 10 hours), amprenavir (16 hours), and TAK-779 (CCR5 antagonist, at 1 hour). At 1, 3, 5, 6, 8, 10, 16, and 20 hours after infection, NOTA was added, and the microplate was incubated for 48 hours at 37 °C with 5% CO_2. After incubation, 100 µL of Bright-Glo luciferase reagent (Promega, Madison, Wisconsin, USA) was added to all wells of the 96-well microplate and aspirated. Then 150 µL from each well was transferred to a 96-well black plate. The Victor Nivo multimode plate reader (Promega, Madison, Wisconsin, USA) was then used to measure the luminescence at 540 nm. The following formula was used to determine the percentage inhibition.

% HIV inhibition = [(average sample – average control)/(1 – (average viral control – average control))] × 100

HIV-1 integrase Assay

The integrase activity of the NOTA compound was evaluated using the HIV-1 Integrase assay (XpressioBio), which is a non-radioactive, calorimetric assay. This assay was done according to the manufacturer's protocol. Briefly, the reaction buffer and blocking solution were pre-heated to 37 °C for 10 minutes. The DS DNA 100x solution was diluted in reaction buffer to create a 1X solution. In the next step, 100 µL of the 1X DS DNA solution was added to each well of the streptavidin-coated 96-well plate and incubated at 37 °C for 30 minutes. Then the sample was removed from the wells and washed five times with 300 uL of 1X wash buffer. 200 µL of blocking buffer was added to each well and further incubated for 30 minutes at 37 °C. For the integrase reaction, the blocking buffer was aspirated, and the wells were washed three times with 200 µL of reaction buffer. The integrase enzyme dilution was prepared according to the kit's recommendations (e.g. 1:300 dilution). 100 µL of diluted enzyme solution was added to the appropriate wells, and the negative control was only reaction buffer. The plate was further incubated for 30 minutes at 37 °C. Following this, the test compound NOTA and the target DNA were added. 50uL of the NOTA (test compound; Raltegravir, sodium azide and reaction buffer for controls) were added to the wells and incubated at room temperature for 5 minutes. Following incubation and washing, 100 µL of Horseradish Peroxidase (HRP) antibody solution was further incubated for 30 minutes at 37 °C. The plate was washed again, and 100 µL of TMB peroxidase substrate was added and incubated for 10 min at room temperature. The absorbance will be measured at 450 nm within 10 minutes of adding the stop solution. By comparing the test article (NOTA) mean absorbance to the integrase-alone control mean absorbance, you may calculate the mean absorbance for each group and find the per cent control activity.

Computational Validation of Zinc Chelation Mechanism: Molecular Docking Studies

Autodock Vina 1.2.5 [51] was employed for molecular docking studies to provide computational validation of the zinc chelation mechanism. The two subtypes, B and C(SA), were prepared (using homology modelling based on their respective sequences as detailed in SI image 3) for docking using a 2-step protocol where hydrogens were added in USCF Chimera 1.1.6,[52] Kollman charges and AutoDock4 atom types definition using AutoDockTools (ADT).[53] The ligand, NOTA, was optimized at a semi-empirical PM6 level and then at the B3LYP/6-31G(d,p) level of theory using Gaussian16[54] and ligand preparation was completed in ADT with torsions assigned. Docking calculations used a 20 × 20 × 20 Å grid box in the N-terminal domain centered on the zinc coordination site (coordinates: x = 155.632 Å, y = 122.315 Å, z = 131.654 Å) with exhaustiveness = 8 and num_modes = 9. For reproducibility, 5 independent docking trials (n=5) were run per system, each trial initiated utilizing different random seeds. The subsequent binding affinities were analyzed using Python 3.12 with NumPy and SciPy libraries, and statistical significance was assessed using two-tailed independent samples t-tests (α = 0.05). AutoDock Vina incorporates zinc coordination parameters known as AutodockZN. It has been shown that empirical scoring continues to underestimate the energetic contributions of Zn-ligand coordination when compared to quantum mechanical methods. [55, 56] This indicates the resulting binding affinities are relative rather than absolute values; however, they do provide comparative analyses and binding mode identification.

Statistical Analysis

The results are presented as the mean ± standard deviation. The significance value was set to $p < 0.05$, and all data included were analysed using an unpaired t-test. The GraphPad Prism 5 software program was used in the data analysis.[57]

RESULTS AND DISCUSSION

In this study, HIV-1 subtype B and subtype C-SA IN enzymes were evaluated, whilst the activity of commercial INSTIs and NOTA against them were compared. Additionally, the utilisation of NOTA as a potential inhibitor of HIV-1 IN was assessed. Analysis of amino acid sequences between IN subtype B and subtype C-SA indicates that these sequences have approximately 93% identity whilst differing at a few positions (Figure S1). Various recombinant techniques were utilized to facilitate the production of highly concentrated HIV-1 IN proteins.[58] Transformation of the HIV-1 IN genes was carried out in the E. coli strain BL21(DE3) and DH5α, although BL21 is accepted as the optimal strain for the expression of recombinant HIV-1 IN.[59] Verification of the HIV-1 IN genes in the isolated plasmids was confirmed by restriction digestion and colony PCR (Figure S2). The HIV-1 IN coding sequences of subtype B and C-SA were mutated to introduce the amino acid substitutions F185K and C280S, which increased IN solubility when expressed in bacteria (Figure S1) without affecting the catalytic activity. [60, 61] The cloned HIV-IN subtype B and C-SA genes in the expression plasmid vector pET302 were successfully expressed in *E. coli* BL21 (DE3) cells. The specified amino acid substitution resulted in increased solubility of both recombinant proteins (Figure 1). Both proteins were successfully purified to >95% homogeneity (Figure 2).

Enzyme kinetics of each subtype were performed in a 96-well plate system using a 38-mer oligonucleotide substrate (5'-[FAM]-ACT GCT AGA GAT TTT CCA CGT GGA AAA TCT CTA GCA GT-[BHQ-1]-3'). A fluorescent signal was produced when IN specifically cleaves the GT dinucleotide, which is linked to the quencher [BHQ-1] at the 3'end.[23] Table 1 shows the summarized kinetic parameters of both subtypes. These parameters indicated that whilst C-SA had a slightly higher K_m value than subtype B, there was an increased catalytic efficiency due to a higher k_{cat} as compared to subtype B (Table 1). The K_m value of 35.54 ± 3.715 nM reported in the study for subtype B is consistent with findings with Smolov *et al.*[9] and Hassounah, *et al.*,[62] as they have reported K_m values of 30 nM and 57 nM, respectively. Notably, the K_m value reported for C-SA lies within the same range at 40.04 ± 9.502 nM.[9, 62] Nevertheless, the K_m values observed do not exhibit a significant difference between subtypes ($p \leq 0.05$).

Subtype B was observed to have a lower catalytic efficiency (k_{cat}/K_m) of 0.0006 ± 0.000 nM^{-1}/s^{-1} and turnover (k_{cat}) number of 0.023 ± 0.004 s^{-1} as compared to subtype C-SA of 0.010 ± 0.005 nM^{-1}/s^{-1} and 0.427 ± 0.020 s^{-1}, respectively (Figure S3). Accordingly, a low k_{cat}

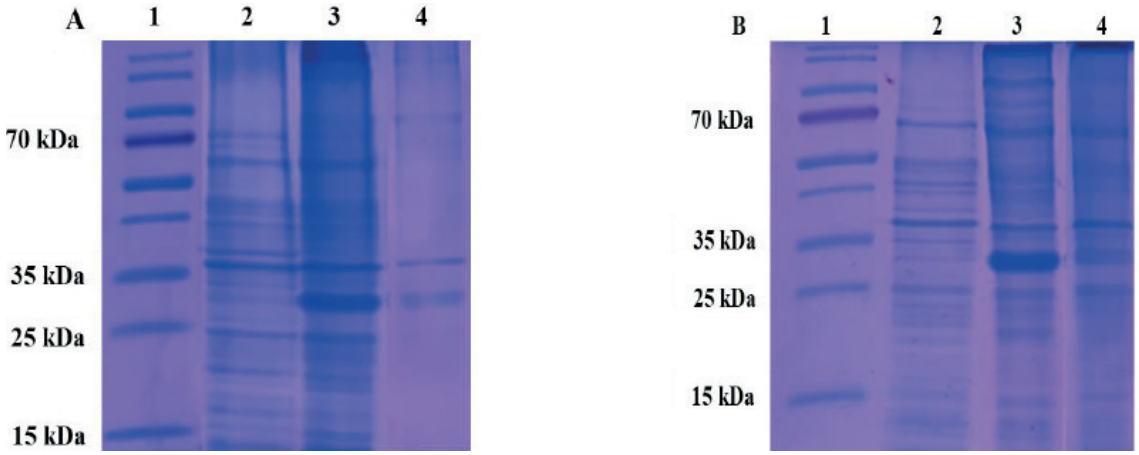


Figure 1: SDS-PAGE verification of expressed HIV-1 IN subtype B (A) and subtype C-SA (B). The gels were stained with brilliant blue Coomassie R-250. (A- B) Lane 1: PageRuler™ Pre-stained protein ladder, Lane 2: Un-induced HIV-1 IN subtype B and C-SA, respectively, Lane 3: Induced HIV-1 IN subtype B and C-SA in the soluble fraction, respectively, Lane 4: Induced HIV-1 IN subtype B and C-SA in the insoluble fraction, respectively. Both proteins migrated with an apparent molecular mass of 32 kDa.

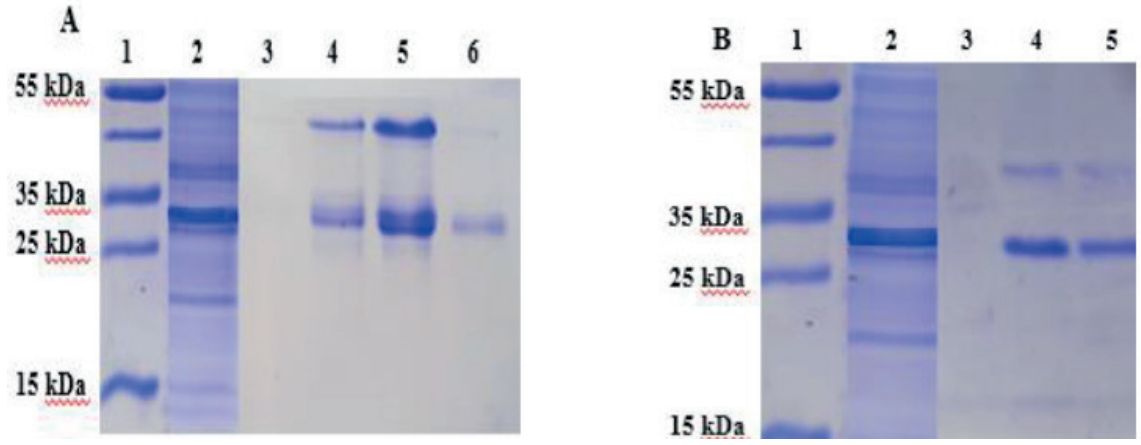


Figure 2: Purification of HIV-1 IN subtype B (A) and subtype C-SA (B) using cobalt affinity chromatography. (A) Lane 1: PageRuler™ Pre-stained protein ladder, Lane 2: Crude subtype B protein, Lane 3: Unbound protein, Lane 4-6: bound proteins. (B) Lane 1: PageRuler™ Pre-stained protein ladder, Lane 2: Crude C-SA protein, Lane 3: Unbound protein, Lane 4-5: bound proteins. The proteins were purified to > 95% homogeneity. Both proteins migrated with an apparent molecular mass of 32 kDa.

Table 1: Comparison of the enzyme kinetic parameters of HIV-1 IN between subtype B and subtype C-SA.

Kinetic Parameters	Subtype B	Subtype C-SA
K_m (nM)	35.5 ± 3.7	40.0 ± 9.502
K_{cat} (S^{-1})	0.023 ± 0.004	0.43 ± 0.020
K_{cat}/K_m (nM^{-1}/S^{-1})	0.0006 ± 0.000	0.010 ± 0.005

Table 2: Analysis of the K_{iapp} obtained from commercial INSTIs and NOTA against HIV-IN Subtype B and C-SA.

Integrase Inhibitors	K_{iapp} (nM)	K_{iapp} (nM)
	Subtype B	Subtype C-SA
Dolutegravir	7.3 ± 0.009	8.3 ± 0.001
Raltegravir	8.2 ± 0.001	9.7 ± 0.004
NOTA	6.8 ± 0.03	8.0 ± 0.2

Experiment conducted in triplicate, $p < 0.05$ = statistically significant. The inhibition produced by the INSTIs was not statistically significant between subtypes B and C ($p = 0.061$)

number suggests that IN remained bound to the DNA even after cleavage, as outlined in the literature.[9, 63] Smolov *et al.*[9] also reported a k_{cat} value of 0.02 min-1, which is in accordance with the results obtained for subtype B. It also suggests that IN remained bound to DNA after cleavage more tightly to subtype B compared to subtype C-SA. This could be attributed to polymorphisms within subtypes, as it affects substrate binding characteristics of IN enzymes.[33, 64] According to Lee *et al.*,[65] the active site for the 3'-processing reaction is equivalent when occurring in the cytoplasm, as the enzyme-viral DNA complex needs to migrate towards the nucleus for strand transfer to occur. Therefore, the HIV-1 IN does not need to turn over after 3'-processing, as only a single copy of the viral DNA is integrated into the host DNA,[63, 64] which is consistent with the findings of our study.

The INSTIs (Dolutegravir and Raltegravir) used in this study are competitive inhibitors.[61] Comparative biochemical tests were conducted to determine the K_{iapp} values ((1), Supplementary Information) for the intrinsic measurement of selected inhibitor potency against HIV-1 IN subtype B and C-SA (Figure S4). Studies based on *in vitro* susceptibilities to purified IN reported K_{iapp} values of HIV-1 INSTIs Dolutegravir and Raltegravir against subtype B in a range of 3.3 nM to 6.7 nM, respectively.[66] This data corresponds to results obtained in this study with values in the range of 6.8 ± 0.03 nM to 9.7 ± 0.004 nM (Table 2). NOTA demonstrated competitive inhibition and exhibited anti-IN activity in the nanomolar range, with greater inhibition and binding affinities towards subtype B in comparison to subtype C-SA. Dolutegravir exhibited stronger inhibition as compared to Raltegravir, as Dolutegravir is a more potent inhibitor, with more robustness against resistance mutations.[62]

The results indicate that NOTA could be utilized as a potential inhibitor against HIV-1. Cytotoxicity studies performed by Ebenhan

et al.[67] functionalized an antimicrobial peptide with NOTA to allow complexation with gallium (68Ga) and was observed to have negligible cytotoxicity. Radiopharmaceuticals that are non-toxic can thus be safely administered to people. Additionally, NOTA had a weak binding affinity to other divalent cations such as magnesium.[67] Nonetheless, under *in vivo* conditions, bioavailability is poor.[30] Therefore, future work will involve attaching NOTA to a suitable carrier, which will improve the INSTI's bioavailability and allow for *in vivo* studies as evidenced in the literature for antimicrobial resistance studies.[31, 68, 69]

The HIV-1 INSTIs and NOTA exhibited weaker inhibition and reduced binding affinities toward subtype C-SA as compared to subtype B. Dolutegravir produced a K_{iapp} of 8.3 ± 0.001 nM in subtype C-SA, compared to subtype B with a K_{iapp} of 7.3 ± 0.009 nM. The inhibitory data from this study are in agreement with other studies that evaluated the K_{iapp} of INSTIs, generating K*iapp* values within a nanomolar range.[70] Raltegravir is reported to have a K_{iapp} value of approximately 6 nM for subtype B, correlating with findings observed in another study.[66] Although subtype B exhibited lower K_{iapp} values and tighter binding of Dolutegravir, Raltegravir, and NOTA, the results indicate that it was not significant when compared to subtype C-SA ($p = 0.061$).

Fluorescence quenching is a useful tool for studying protein and drug interactions.[45] Once the protein interacts with other compounds, its intrinsic fluorescence usually varies. HIV-1 IN contains four tryptophan (Trp) residues near the active site, which emit fluorescence.[32, 33] The change in fluorescence observed between both subtype B and C-SA signifies the interaction between both of those proteins with the INSTIs and the chelating agent. The quenching of fluorescence intensity can transpire by different mechanisms.[71] The thermodynamic parameters of INSTIs and NOTA binding to HIV-1 subtype B and subtype C-SA were compared *via* fluorescence quenching, using Stern-Volmer plots ((2), Supplementary Information) for analysis. The Stern-Volmer quenching constant (K_{sv}) from the slope of a linear regression plot, depicted increasing K_{sv} values with the utilization of higher temperatures for both subtype B and subtype C-SA (Figure 3). This is indicative of dynamic quenching and provides information on the overall conformational changes of the active site.

All integrase inhibitors studied possessed a higher K_{sv} against subtype B when compared to C-SA. The chelating agent NOTA displayed the best K_{sv} against subtype B and subtype C-SA, with a K_{sv} of 15.30 ± 0.14 µM and 14.20 ± 0.18 µM, respectively (Table 3). Thus, an observed correlation between the data in Table 2 (K_i) and Table 3 (K_{sv}) can be noted. Although these results were not significant in comparison to the commercial inhibitors, Raltegravir and Dolutegravir.

To determine how interactional forces function between the INSTIs and the IN subtypes B and C-SA, temperature-dependent thermodynamics parameters for the interaction between the ligand and the enzyme were analysed per the Van't Hoff equation ((3), Supplementary Information).

Thermodynamic parameters (Table 4), including enthalpy (ΔH) and entropy (ΔS), were determined for the INSTIs and NOTA (4), Supplementary Information. As competitive inhibitors, Raltegravir and Dolutegravir inhibit retroviral integration; hence, their potency is directly related to the affinity with which they bind the IN molecule.[46] In addition, it was observed that for both subtypes, the Gibbs free energy (ΔG) was negative. This indicates that there is a change of system free energy between the protein-ligand, and binding occurs spontaneously. Although all integrase inhibitors bound efficiently to both IN subtypes, better binding affinities were observed with subtype B, and this was influenced by the binding entropy. NOTA had the highest Gibbs free energy against subtype B with -9.8 kcal/mol and subtype C-SA with -9.7 kcal/mol (Table 4).

A study by Hutapea and Maladan[72] reported the binding affinity of HIV-1 INSTIs against subtype B at -7.8 kcal/mol, whilst Isaacs *et al.*[73] also observed binding affinities against subtype B at -4.4 kcal/mol for Raltegravir and -3.4 kcal/mol for Dolutegravir, respectively. Notably, ΔH was positive for all drugs, whilst all integrase-inhibitor interactions were entropy-driven, denoted by the high negative -TΔS values obtained.

The antiviral activity of the NOTA, raltegravir, dolutegravir and elvitegravir was assessed on TZM-bl cell lines infected with HIV-1 subtype B and C using the luciferase-based antiviral assay (Figure 5). The results showed that NOTA can successfully inhibit HIV-1 subtype C and B. At the highest utilized concentration, NOTA showed 84% HIV subtype B inhibition with an IC_{50} of 20.91 ug/mL. Using the same concentration of NOTA, 97% inhibition was achieved against HIV subtype C, with an IC_{50} of 0.07946 ug/mL. These results indicate that

Table 3: Stern-Volmer quenching constants (K_{sv}) at 298 K of HIV-1 IN subtype B and subtype C-SA after their interaction with INSTIs and NOTA

Integrase Inhibitors	K_{sv} (μM^{-1}) at 298 K	K_{sv} (μM^{-1}) at 298 K
	Subtype B	Subtype C-SA
Dolutegravir	11.9 ± 0.05	10.1 ± 0.03
Raltegravir	12.9 ± 0.02	11.2 ± 0.04
NOTA	15.3 ± 0.14	14.2 ± 0.18

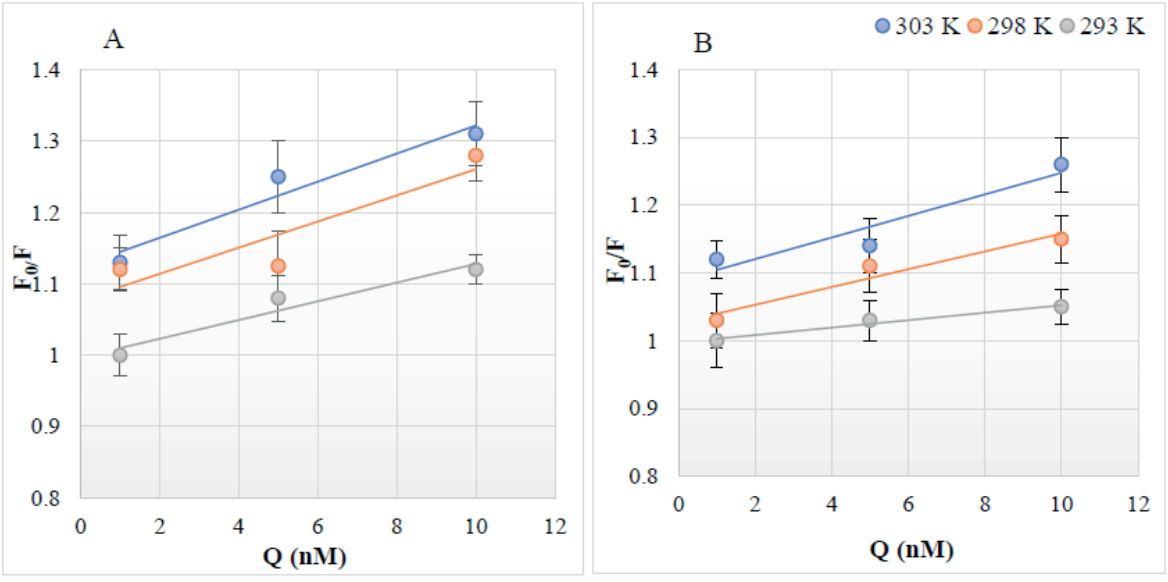


Figure 3: Stern-Volmer plots for fluorescence quenching of HIV-1 IN subtype B (A) and subtype C-SA (B). The final volume of 100 µL was treated with Raltegravir at various temperatures at 293 K, 298 K, and 303 K (n =3).

Table 4: Analysis of thermodynamic parameters for INSTIs and NOTA

Integrase Inhibitors	Integrase	Parameter		
		ΔG (kcal/mol)	ΔH (kcal/mol)	TΔS (kcal/mol)
Dolutegravir	Subtype B	-9.4	-43.2	-52.9
	Subtype C-SA	-9.7	-25.7	-35.3
Raltegravir	Subtype B	-9.7	-8.1	-17.8
	Subtype C-SA	-9.6	-9.3	-18.9
NOTA	Subtype B	-9.8	-37.6	-47.4
	Subtype C-SA	-9.7	-35.6	-45.3

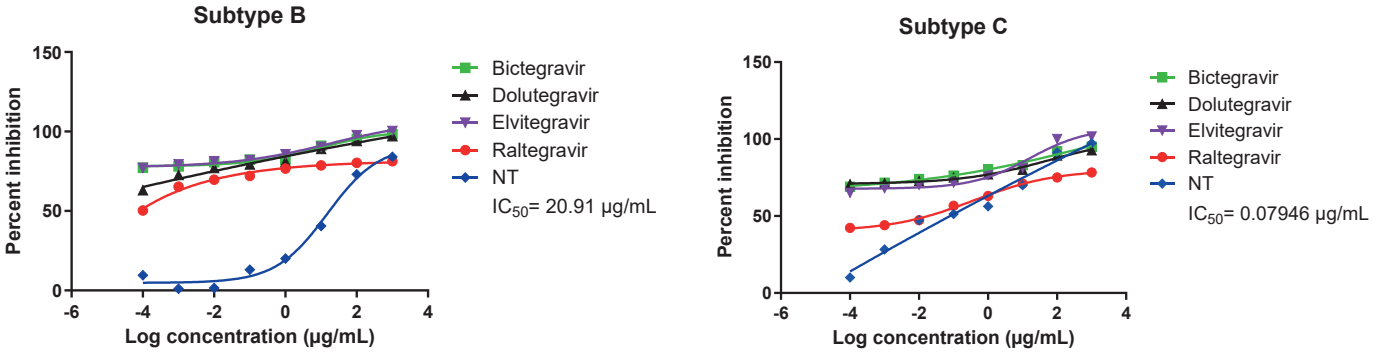


Figure 5. HIV-1 Inhibition curve of NOTA. **A**: The inhibition of HIV-1 subtype B **B:** The inhibition of HIV-1 subtype C. The positive controls were: Bictegravir (green), Dolutegravir (black), Elvitegravir (purple) and Raltegravir (red).

NOTA inhibits HIV-1 subtype C with greater affinity than subtype B. In Figure 5, for HIV-1 subtype B, the percentage of inhibition for Bictegravir, Elvitegravir, Dolutegravir and Raltegravir were 98%, 100%, 97% and 81%, respectively. For HIV-1 subtype C, the percentage of inhibition for Bictegravir, Elvitegravir, Dolutegravir and Raltegravir were 95%, 100%, 93% and 78%, respectively. The percentage inhibition and IC_{50} of Bictegravir, Elvitegravir, Dolutegravir, and NOTA for subtype C, thus fell within a similar range of 93 – 100%, indicating that NOTA's activity correlates well with commercial INSTIs.NOTA is potentially more effective at inhibiting HIV-1 subtype C due to HIV-1 subtype C possibly having a lower genetic barrier to susceptibility against integrase inhibition. The IC_{50} of Dolutegravir was 0.0001 µg/mL for both subtype B and C. The IC_{50} of Raltegravir was 0.00009 µg/mL for subtype B and 0.01755 µg/mL for subtype C. Raltegravir may be more effective at inhibiting subtype B and C due to potential genetic differences driving the susceptibility in subtype B or resistance in subtype C.

The key stages in the life cycle of HIV occur during attachment (0-1 hours), reverse transcription (3-8 hours), integration (6-12 hours) and proteolysis (16-24 hours). The principle behind the time of addition assay is to determine at which stage of the life cycle inhibition occurs. For the integration stage, dolutegravir, raltegravir, bictergravir and elvitegravir were used. NOTA was added at all the time points concurrently with the controls. Figure 6 showed that NOTA maintained more than 50% HIV-1 inhibition during 8-12 hours, which correlated with the integration stage of the life cycle. Bictegravir, elvitegravir and raltegravir maintained > 50% inhibition, with only dolutegravir exhibiting < 50% inhibition at 10 hours. The controls are integrase strand transfer inhibitors. NOTA showed 78% HIV inhibition during integration for subtype C. This suggests that NOTA has less inhibitory effects in HIV-1 subtype B when compared to subtype C. NOTA had low cytotoxicity and inhibited the viral replication of HIV integration. Using immortalized cell lines, the IC_{50} of NOTA showed greater potency toward HIV-1 subtype C than B. The time of addition experiments demonstrated that NOTA blocks the late stage of reverse transcription (nuclear import) until the late stage of HIV integration (6-10 hours). In this assay, it was also noted that a lag period before inhibition exists; therefore, future animal studies could be performed to determine the *in vivo* time to inhibition.

Furthermore, the activity of NOTA was tested in the integrase activity assay (Figure 7). The IN activity assay indicated that NOTA inhibited the integration by 60 %. The reference control Raltegravir had a lower IC_{50} compared to NOTA. However, NOTA inhibited integrase activity over 50% utilising a broader concentration range, as compared to Raltegravir. The integrase activity was based on HIV-1 subtype B. This assay measures the ability of a compound to block HIV-1 integrase's strand transfer step, which is essential for integrating viral DNA into the host genome. This assay is a normal calorimetric test. Integrase inhibitors may also act by blocking the 3'processing step or nuclear import step. The 3'-processing inhibitor activity assay measured the compound's ability to block the crucial 3'-end processing step during viral DNA integration. This involves incubating a labelled viral LTR or DNA substrate with the enzyme and inhibitor, followed by measuring the inhibition of the 3'-nucleotide removal step through real-time PCR methods.[74] These results suggest that NOTA inhibits the IN activity by either strand transfer or nuclear import.

Molecular docking was performed using AutoDock Vina 1.2 employing the AutoDock4Zn force field, a zinc-specific scoring function developed and validated on 292 zinc metalloprotein crystal complexes[75] that accurately models the energetic and geometric components of zinc-ligand coordination. While all-atomistic MD simulations can provide equilibrium and long-timescale binding information, the AutoDock4Zn force field within Vina was used for the validated prediction of NOTA binding poses at the NTD zinc site. This is consistent with established protocols for zinc-coordinating ligand docking. The HHCC zinc finger coordination geometry requires atomistic-level resolution that coarse-grained methods cannot provide, as current CG force fields, such as Martini, lack parameterisation for zinc ions. Extended all-atomistic MD analyses of this system, employing enhanced-sampling methods, are currently ongoing in our laboratories. Molecular docking studies were carried out to provide a structural context into NOTA mediated Zn chelation in HIV-1 integrase at the N-terminal domain (NTD) zinc coordination sites. Five independent docking trials showed comparable binding affinities for NOTA at Zinc site 1 and site 2 in both HIV-1 Subtype B wild-type (ΔG = -5.98 ± 0.045 kcal/mol) vs subtype C South African variant (ΔG = -6.00 ± 0.000 kcal/mol). There was a negligible statistical

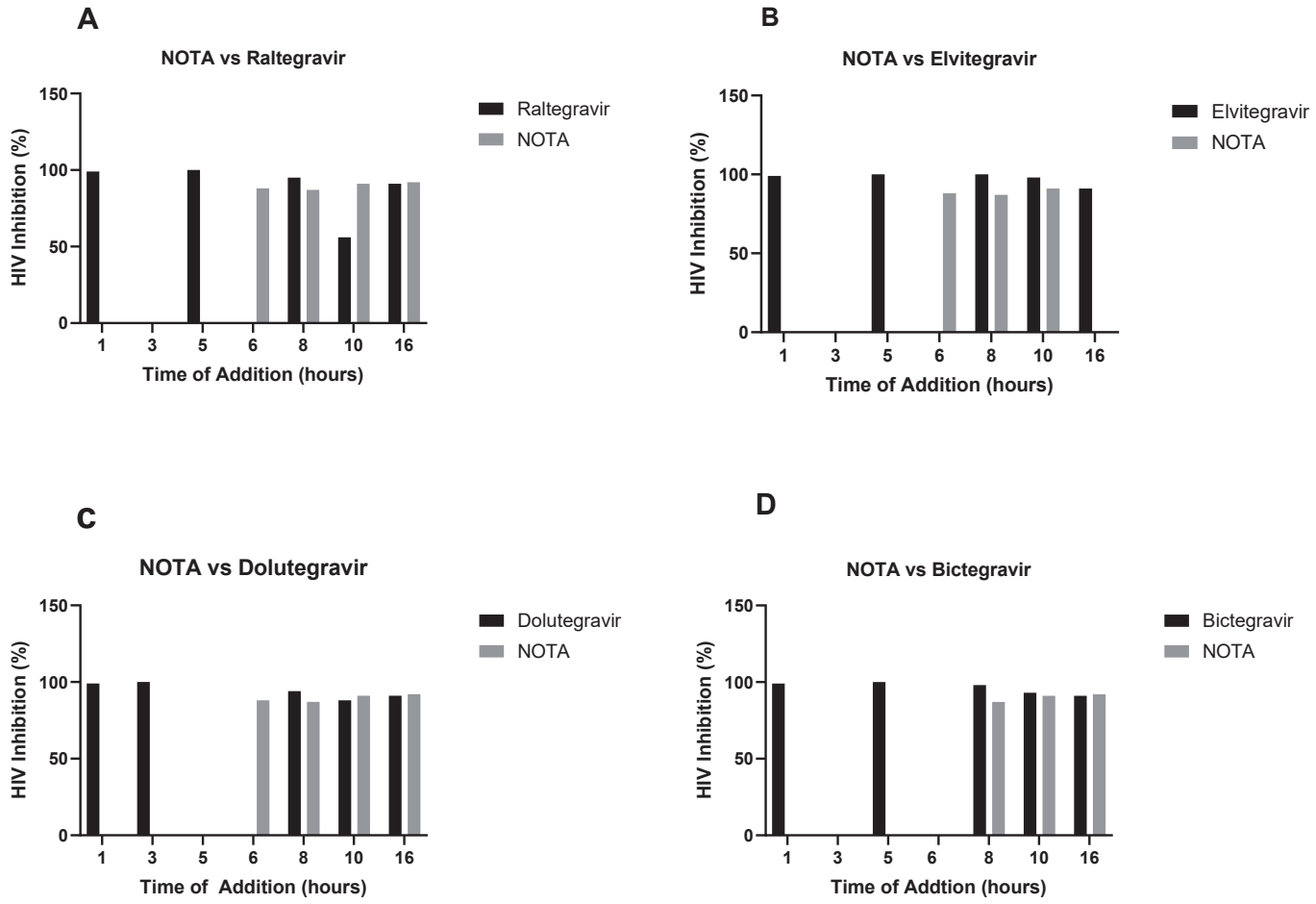


Figure 6. Time of addition assay to confirm that NOTA inhibit the HIV-1 integration. A) indicate the time of addition assay using HIV-1 subtype C and B) HIV-1 subtype B

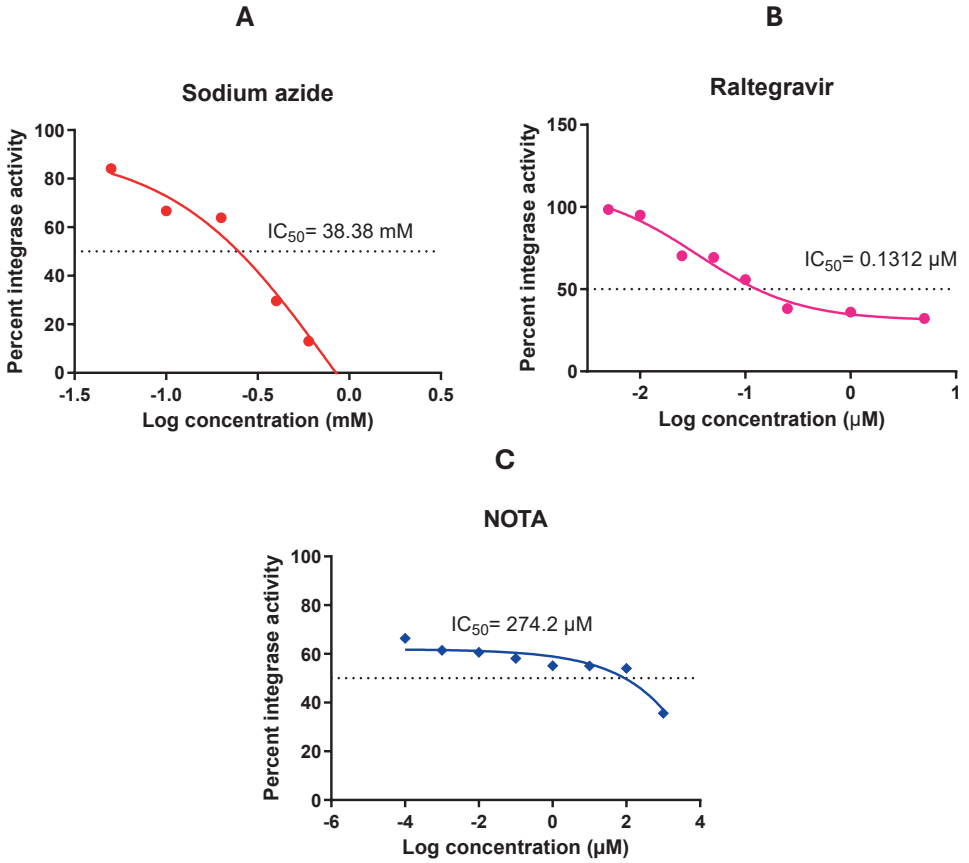


Figure 7: Strand transfer Integrase activity assay. Integrase inhibitors, controls and INSTIs representing a concentration range generated from a five-fold serial dilution. A) Sodium azide (assay control), B.) Raltegravir and C.) NOTA

difference between the subtypes ($p = 0.347$, two-tailed t-test). Energy landscape results (Figure S3) illustrate excellent reproducibility across trials and a 1% coefficient of variation, as shown in Table 5.

The predicted binding modes with (interatomic distances between N/O and Zn) place NOTA's triazacyclononane ring nitrogen atoms within 5.6 Å of the zinc ion (N1-Zn: ~4.2-4.3 Å, N4-Zn: ~5.0-5.1 Å, N7-Zn: ~5.4-5.5 Å), with the nearest carboxylate oxygen/nitrogen at approximately 5.6 Å, consistent with hexadentate chelation geometry (Figures 8 and 9).

Representative binding pose of NOTA at the HIV-1 Subtype B (wild-type) integrase N-terminal domain Zinc Site 1, showing the most favourable predicted binding mode (Mode 1, ΔG = -5.98 kcal/mol) NOTA is displayed in stick representation with the triazacyclononane ring (carbon atoms in gray, nitrogen atoms in blue) and three carboxylate arms (oxygen atoms in red). Interatomic distances between zinc and NOTA donor atoms are shown as red lines for oxygen and blue for nitrogen in angstroms with distance labels. The closest donor is at approximately 5.6 Å (N1-Zn: 5.6 Å), indicating comparable chelation potential. The structural similarity between WT and C(SA) binding modes supports the observed lack of significant difference in binding affinity ($p = 0.347$) and suggests pan-subtype efficacy of NOTA-based zinc chelation. The docking studies showed a stronger binding affinity in comparison to zinc site 2 for both systems ($p < 0.001$), demonstrating possible site selectivity. The calculations support the experimental findings of pan-subtype inhibitory activity in this study and give structural validation for NOTA mediated zinc chelation. While the docking predicted binding affinities (-5.98 to -6.00 kcal/mol) are lower in magnitude vs the experimental, this disparity is not out of line, given the known limitations of empirical scoring functions in accurately simulating metal coordination energies.[55]

The enzyme competitive model of IN represented herein provided the best statistical fit to the kinetic data. However, the inhibition is mechanistically interpreted as indirect competition through the disruption of enzyme functionality. This interpretation is consistent with the docking data showing NOTA binding at the NTD, the time-of-addition results, and previous reports demonstrating the importance of zinc-dependent multimerisation for integrase activity.[12, 76]

CONCLUSION

HIV-1 subtype B had a higher affinity for the oligonucleotide substrate, whilst the catalytic efficiency is intrinsically slower as compared to subtype C-SA. Competitive inhibition studies utilizing Dolutegravir, Raltegravir, and NOTA indicated that these drugs exhibited reduced inhibitory activity and affinity to subtype C-SA, as compared to subtype B). Subsequently, the drugs exhibited greater negative ΔG values against subtype B in comparison to subtype C-SA. HIV-1 IN function was similar in both subtypes; however, based on the binding affinity of NOTA as compared to INSTIs, this chelating agent demonstrated superior activity. Molecular docking of HIV-1 subtype B and C(SA) provided structural validation, with no significant difference between the two subtypes, indicating favourable binding energies for zinc chelation. Overall, NOTA demonstrated comparable activity to the INSTIs. It is proposed that conjugation of NOTA to a suitable bioavailable carrier may enhance its inhibitory potency against HIV-1 integrase subtypes B and C-SA. The incorporation of advanced delivery strategies, such as nanoparticle-based systems or intranasal administration, could further improve drug penetration and absorption, particularly within the central nervous system. Future studies should therefore focus on evaluating the in vivo efficacy of NOTA-based formulations to better understand its therapeutic potential. In addition, the ability of NOTA to target metal-dependent integrase sites suggests broader applicability, and its activity against other viruses possessing metallo-based integrases warrants further investigation.

Table 5: AutoDock Vina Binding Affinities for NOTA at HIV-1 Integrase Zinc Sites

System	Mean (kcal/mol)	SD	p-value vs WT Zn1
HIV-1 C(SA) Zn1	-6.00	0.000	0.347 (ns)
HIV-1 WT Zn1	-5.98	0.045	-
HIV-1 WT Zn2	-5.90	0.000	<0.001 ***
HIV-1 C(SA) Zn2	-5.82	0.045	<0.001 ***

Values represent mean ± standard deviation (SD) from five independent docking trials ($n = 5$ per system). Statistical comparisons were performed using two-tailed independent samples t-tests. ns = not significant; ***$p < 0.001$. Complete raw data for all binding modes are provided in the Supplementary Information: Table S1-4.

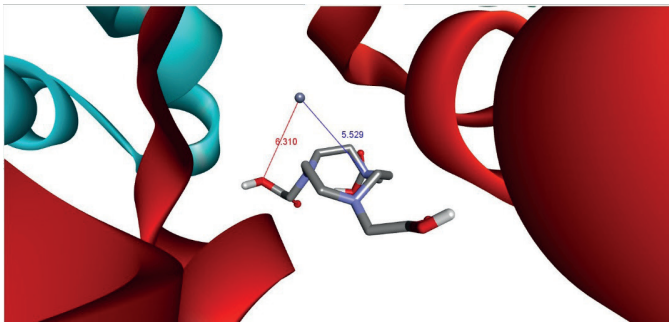


Figure 8: Best Binding Mode - HIV-1 Subtype B (Wild-Type) Zinc Site 1.

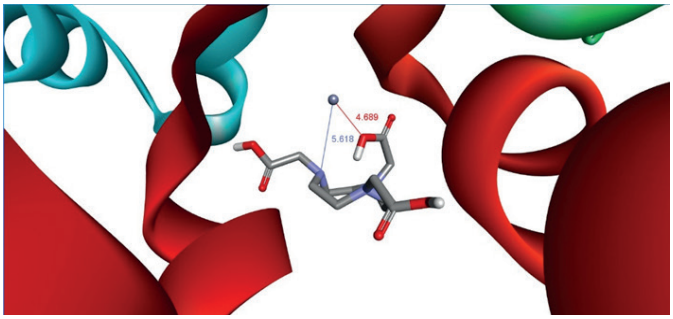


Figure 9: Best Binding Mode - HIV-1 Subtype C (South African) Zinc Site 1. Representative binding pose of NOTA at the HIV-1 Subtype C (South African) integrase N-terminal domain Zinc Site 1, showing the most favourable predicted binding mode (Mode 1, ΔG = -6.00 kcal/mol). NOTA is displayed in stick representation with the triazacyclononane ring (carbon atoms in gray, nitrogen atoms in blue) and three carboxylate arms (oxygen atoms in red). Interatomic distances between zinc and NOTA donor atoms are shown as red lines for Oxygen and blue for Nitrogen with distances shown in angstroms. The three nitrogen atoms from the NOTA ring are positioned at distances less than 5.6 Å from the zinc centre (N1-Zn: 5.6 Å), consistent with zinc coordination geometry. The closest carboxylate oxygen is at approximately 4.7 Å, suggesting a potential chelation interaction. This binding mode demonstrates NOTA's hexadentate chelating capability with favourable positioning for zinc extraction from the HHCC coordination sphere.

SUPPLEMENTARY INFORMATION

The supporting information includes additional figures and equations, used to obtain the preliminary results. The identification of resistance genes from the sequence alignment (Figure S1), verification of HIV integrase (Figure S2), HIV-1 integrase 3' processing activity assay (Figure S3), inhibition studies (Figure S4), and molecular docking studies (Table S1-4, Figure S5).

ACKNOWLEDGEMENTS

We thank the National Research Foundation and the University of KwaZulu-Natal, College of Health Sciences, for financial support.

CREDIT AUTHORSHIP CONTRIBUTIONS STATEMENT

Hendrik G. Kruger conceptualised the idea and designed the project with Glenn E. M. Maguire, Tricia Naicker, Thavendran Govender and Johnson Lin. Nakita Reddy performed the data analysis and interpretation, and wrote and compiled the manuscript. Kevyna Chetty, Sibusiso Maseko, Darian Naidu, Charmaine Kahiye, and Nompumelelo Mkhwanazi performed the experiments and wrote parts of the manuscript. All authors contributed to revising the manuscript for intellectual content.

DECLARATION OF COMPETING OR FINANCIAL INTERESTS

The authors declare that they have no known competing financial interests or personal relationships that could have influenced the work reported in this paper.

DECLARATION OF GENERATIVE AI AND AI-ASSISTED TECHNOLOGIES

The authors declare that no generative AI or AI-assisted technologies were used for the purpose of the research conducted or for the preparation of the manuscript.

AUTHORS ORCID

Nakita Reddy: https://orcid.org/0000-0003-4428-2241
Sibusiso Maseko: https://orcid.org/0000-0001-7025-6106
Charmaine Kahiya: https://orcid.org/0000-0003-1554-875X
Glenn E. M. Maguire: https://orcid.org/0000-0002-9135-5370
Tricia Naicker: https://orcid.org/0000-0002-7134-6258
Thavendran Govender: https://orcid.org/0000-0003-2511-2503
Johnson Lin: https://orcid.org/0000-0002-9621-9343
Nompumelelo P. Mkhwanazi: https://orcid.org/0000-0002-0808-9201
Hendrik G. Kruger: https://orcid.org/0000-0003-0606-2053

REFERENCES

1. UNAIDS. UNAIDS Fact Sheet. https://www.unaids.org/en/resources/fact-sheet (accessed July 2024).
2. Alan E, Peter C. Retroviral Integrase Structure and DNA Recombination Mechanism. Mob DNA. 2015;III:1011–1033. https://doi.org/10.1128/9781555819217.ch44.
3. Brado D, Obasa AE, Ikomey GM, Cloete R, Singh K, Engelbrecht S, Neogi U, Jacobs GB. Analyses of Hiv-1 Integrase Sequences Prior to South African National Hiv-Treatment Program and Availability of Integrase Inhibitors in Cape Town, South Africa. Sci Rep. 2018;8(1):4709. https://doi.org/10.1038/s41598-018-22914-5.
4. Auvert B, Males S, Puren A, Taljaard D, Caral M, Williams B. Can Highly Active Antiretroviral Therapy Reduce the Spread of HIV? J Acquir Immune Defic Syndr. 2004;36(1):613–621. https://doi.org/10.1097/00126334-200405010-00010.
5. Foka FET, Mufhandu HT. Current Arts, Virologic Failure, and Implications for Aids Management: A Systematic Review. Viruses. 2023;15(8):1732. https://doi.org/10.3390/v15081732.
6. Delelis O, Carayon K, Saïb A, Deprez E, Mouscadet J-F. Integrase and Integration: Biochemical Activities of Hiv-1 Integrase. Retrovirology. 2008;5(1):114. https://doi.org/10.1186/1742-4690-5-114.
7. Craigie R. Hiv Integrase, a Brief Overview from Chemistry to Therapeutics. J Biol Chem. 2001;276(26):23213–23216. https://doi.org/10.1074/jbc.R100027200.
8. Mori M, Kovalenko L, Lyonnais S, Antaki D, Torbett BE, Botta M, Mirambeau G, Mély Y. Nucleocapsid Protein: A Desirable Target for Future Therapies against HIV-1. In: Torbett BE, Goodsell DS, Richman DD (editors), The Future of HIV-1 Therapeutics. Current Topics in Microbiology and Immunology, Vol 389. Cham: Springer; 2015. pp. 53–92. https://doi.org/10.1007/82_2015_433.
9. Smolov M, Gottikh M, Tashlitskii V, Korolev S, Demidyuk I, Brochon JC, Mouscadet JF, Deprez E. Kinetic study of the HIV−1 DNA 3'-end processing. FEBS J. 2006;273(6):1137–1151. https://doi.org/10.1111/j.1742-4658.2006.05139.x.
10. Pannecouque C, Szafarowicz B, Volkova N, Bakulev V, Dehaen W, Mély Y, Daelemans D. Inhibition of Hiv-1 Replication by a Bis-Thiadiazolbenzene-1, 2-Diamine That Chelates Zinc Ions from Retroviral Nucleocapsid Zinc Fingers. Antimicrob Agents Chemother. 2010;54(4):1461–1468. https://doi.org/10.1128/AAC.01671-09.
11. Eilers G, Gupta K, Allen A, Zhou J, Hwang Y, Cory MB, Bushman FD, Van Duyne G. Influence of the Amino-Terminal Sequence on the Structure and Function of Hiv Integrase. Retrovirology. 2020;17(1):28. https://doi.org/10.1186/s12977-020-00537-x.
12. Zheng R, Jenkins TM, Craigie R. Zinc folds the N-terminal domain of HIV-1 integrase, promotes multimerization, and enhances catalytic activity. Proc Natl Acad Sci USA. 1996;93(24):13659–13664. https://doi.org/10.1073/pnas.93.24.13659.
13. Summa V, Petrocchi A, Bonelli F, Crescenzi B, Donghi M, Ferrara M, Fiore F, Gardelli C, Gonzalez Paz O, Hazuda DJ, et al. Discovery of Raltegravir, a Potent, Selective Orally Bioavailable Hiv-Integrase Inhibitor for the Treatment of Hiv-Aids Infection. J Med Chem. 2008;51(18):5843–5855. https://doi.org/10.1021/jm800245z.
14. Shimura K, Kodama E, Sakagami Y, Matsuzaki Y, Watanabe W, Yamataka K, Watanabe Y, Ohata Y, Doi S, Sato M, et al. Broad Antiretroviral Activity and Resistance Profile of the Novel Human Immunodeficiency Virus Integrase Inhibitor Elvitegravir (Jtk-303/Gs-9137). J Virol. 2008;82(2):764–774. https://doi.org/10.1128/JVI.01534-07.
15. Demarest J, Underwood M, St. Clair M, Dorey D, Brown D, Zolopa A. Short Communication: Dolutegravir-Based Regimens Are Active in Integrase Strand Transfer Inhibitor–Naive Patients with Nucleoside Reverse Transcriptase Inhibitor Resistance. AIDS Res Hum Retroviruses. 2018;34(4):343–346. https://doi.org/10.1089/aid.2017.0184.
16. Hill L, Smith SR, Karris MY. Profile of Bictegravir/Emtricitabine/Tenofovir Alafenamide Fixed Dose Combination and Its Potential in the Treatment of Hiv-1 Infection: evidence to Date. HIV AIDS (Auckl). 2018;10:203–213. https://doi.org/10.2147/HIV.S145529.
17. Shamu P, Mullick S, Christofides NJ. Perceptions of the Attributes of New Long-Acting Hiv Pre-Exposure Prophylaxis Formulations Compared with a Daily, Oral Dose among South African Young Women: A Qualitative Study. AIDS Care. 2024;36(12):1815–1825. https://doi.org/10.1080/09540121.2024.2383878.
18. Mataboge P, Nzenze S, Mthimkhulu N, Mazibuko M, Kutywayo A, Butler V, Naidoo N, Mullick S. Planning for Decentralized, Simplified Prep: Learnings from Potential End Users in Ga-Rankuwa, Gauteng, South Africa. Front Reprod Health. 2023;4:1081049. https://doi.org/10.3389/frph.2022.1081049.
19. Passos DO, Li M, Yang R, Rebensburg SV, Ghirlando R, Jeon Y, Shkriabai N, Kvaratskhelia M, Craigie R, Lyumkis D. Cryo-Em Structures and Atomic Model of the Hiv-1 Strand Transfer Complex Intasome. Science. 2017;355(6320):89–92. https://doi.org/10.1126/science.aah5163.
20. Maertens GN, Hare S, Cherepanov P. The Mechanism of Retroviral Integration from X-Ray Structures of Its Key Intermediates. Nature. 2010;468(7321):326–329. https://doi.org/10.1038/nature09517.
21. Balakrishnan M, Yant SR, Tsai L, O'Sullivan C, Bam RA, Tsai A, Niedziela-Majka A, Stray KM, Sakowicz R, Cihlar T. Non-Catalytic Site Hiv-1 Integrase Inhibitors Disrupt Core Maturation and Induce a Reverse Transcription Block in Target Cells. PLoS One. 2013;8(9):e74163. https://doi.org/10.1371/journal.pone.0074163.
22. Jurado KA, Engelman A. Multimodal Mechanism of Action of Allosteric Hiv-1 Integrase Inhibitors. Expert Rev Mol Med. 2013;15:e14. https://doi.org/10.1017/erm.2013.15.
23. Dick A, Cocklin S. Recent Advances in Hiv-1 Gag Inhibitor Design and Development. Molecules. 2020;25(7):1687. https://doi.org/10.3390/molecules25071687.
24. Rice WG, Schaeffer CA, Harten B, Villinger F, South TL, Summers MF, Henderson LE, Bess JW Jr, Arthur LO, McDougal JS, et al. Inhibition of Hiv-1 Infectivity by Zinc-Ejecting Aromatic C-Nitroso Compounds. Nature. 1993;361(6411):473–475. https://doi.org/10.1038/361473a0.
25. Rice W, Turpin J. Virus-Encoded Zinc Fingers as Targets for Antiviral Chemotherapy. Rev Med Virol. 1996;6(4):187–199. https://doi.org/10.1002/(SICI)1099-1654(199612)6:4<187::AID-RMV176>3.0.CO;2-F.
26. Turpin JA, Song Y, Inman JK, Huang M, Wallqvist A, Maynard A, Covell DG, Rice WG, Appella E. Synthesis and Biological Properties of Novel

Pyridinioalkanoyl Thiolesters (Pate) as Anti-Hiv-1 Agents That Target the Viral Nucleocapsid Protein Zinc Fingers. J Med Chem. 1999;42(1):67–86. https://doi.org/10.1021/jm9802517.

27. Miller Jenkins LM, Byrd JC, Hara T, Srivastava P, Mazur SJ, Stahl SJ, Inman JK, Appella E, Omichinski JG, Legault P. Studies on the Mechanism of Inactivation of the Hiv-1 Nucleocapsid Protein Ncp7 with 2-Mercaptobenzamide Thioesters. J Med Chem. 2005;48(8):2847–2858. https://doi.org/10.1021/jm0492195.
28. Khatib O, Alshimale T, Alsaadi A, Thallaj N. The Global Impact of Hiv: A Comprehensive. Int. J. Adv. Pharm. Sci. Res. 2024;4(3):6–19. https://doi.org/10.54105/ijapsr.C4040.04030424.
29. Somboro AM, Tiwari D, Bester LA, Parboosing R, Chonco L, Kruger HG, Arvidsson PI, Govender T, Naicker T, Essack SY. Nota: A Potent Metallo-β-Lactamase Inhibitor. J Antimicrob Chemother. 2015;70(5):1594–1596. https://doi.org/10.1093/jac/dku538.
30. Omolabi KF, Reddy N, Mdanda S, Ntshangase S, Singh SD, Kruger HG, Naicker T, Govender T, Bajinath S. The in Vitro and in Vivo Potential of Metal-Chelating Agents as Metallo-Beta-Lactamase Inhibitors against Carbapenem-Resistant Enterobacterales. FEMS Microbiol Lett. 2023;370:fnac122. https://doi.org/10.1093/femsle/fnac122.
31. Peters BK, Reddy N, Shungube M, Girdhari L, Baijnath S, Mdanda S, Chetty L, Ntombela T, Arumugam T, Bester LA, et al. In Vitro and in Vivo Development of a β-Lactam-Metallo-β-Lactamase Inhibitor: Targeting Carbapenem-Resistant Enterobacterales. ACS Infect Dis. 2023;9(3):486–496. https://doi.org/10.1021/acsinfecdis.2c00485.
32. Okoye NC, Baumeister JE, Najafi Khosroshahi F, Hennkens HM, Jurisson SS. Chelators and Metal Complex Stability for Radiopharmaceutical Applications. Radiochim Acta. 2019;107(9-11):1087–1120. https://doi.org/10.1515/ract-2018-3090.
33. Bar-Magen T, Sloan RD, Faltenbacher VH, Donahue DA, Kuhl BD, Oliveira M, Xu H, Wainberg MA. Comparative Biochemical Analysis of Hiv-1 Subtype B and C Integrase Enzymes. Retrovirology. 2009;6(1):103. https://doi.org/10.1186/1742-4690-6-103.
34. Bekker L-G, Beyrer C, Mgodi N, Lewin SR, Delany-Moretlwe S, Taiwo B, Masters MC, Lazarus JV. Hiv Infection. Nat Rev Dis Primers. 2023;9(1):42. https://doi.org/10.1038/s41572-023-00452-3.
35. Hemelaar J. Implications of Hiv Diversity for the Hiv-1 Pandemic. J Infect. 2013;66(5):391–400. https://doi.org/10.1016/j.jinf.2012.10.026.
36. He H, Ma X, Liu B, Zhang X, Chen W, Wang C, Cheng S. High-throughput real-time assay based on molecular beacons for HIV-1 integrase 3'-processing reaction. Acta Pharmacol Sin. 2007;28(6):811–817. https://doi.org/10.1111/j.1745-7254.2007.00561.x.
37. Lee PY, Costumbrado J, Hsu C-Y, Kim YH. Agarose Gel Electrophoresis for the Separation of DNA Fragments. J Vis Exp. 2012;62:e3923. https://doi.org/10.3791/3923.
38. Marcus-Sekura CJ, Woerner AM, Zweig M, Court DL, Levin JG, Klutch M. Expression of Hiv-1 Integrase in E. Coli: Immunological Analysis of the Recombinant Protein. AIDS Res Hum Retroviruses. 1990;6(12):1399–1408. https://doi.org/10.1089/aid.1990.6.1399.
39. Lee D-H, Hyun U-S, Kim J-Y, Shin C-G. Characterization of Biochemical Properties of Feline Foamy Virus Integrase. J Microbiol Biotechnol. 2010;20(6):968–973. https://doi.org/10.4014/jmb.1003.03006.
40. Maseko SB, Padayachee E, Govender T, Sayed Y, Kruger G, Maguire GE, Lin J. I36t↑ T Mutation in South African Subtype C (C-Sa) Hiv-1 Protease Significantly Alters Protease-Drug Interactions. Biol Chem. 2017;398(10):1109–1117. https://doi.org/10.1515/hsz-2017-0107.
41. Gasteiger E, Hoogland C, Gattiker A, Duvaud S, Wilkins MR, Appel RD, Bairoch A. Protein Identification and Analysis Tools on the ExPASy Server. In: Walker JM (editor), The Proteomics Protocols Handbook. Springer Protocols Handbooks. Totowa: Humana Press; 2005. https://doi.org/10.1385/1-59259-890-0:571.
42. Graham DR, Garnham CP, Fu Q, Robbins J, Van Eyk JE. Improvements in Two-Dimensional Gel Electrophoresis by Utilizing a Low Cost "in-House" Neutral Ph Sodium Dodecyl Sulfate-Polyacrylamide Gel Electrophoresis System. Proteomics. 2005;5(9):2309–2314. https://doi.org/10.1002/pmic.200401249.
43. Park KH, Kim M, Bae SE, Lee HJ, Kim K-C, Choi BS, Kim YB. Study on Suitable Analysis Method for Hiv-1 Non-Catalytic Integrase Inhibitor. Virol J. 2021;18(1):17. https://doi.org/10.1186/s12985-020-01476-x.
44. Schlamadinger DE, Kats DI, Kim JE. Quenching of Tryptophan Fluorescence in Unfolded Cytochrome C: A Biophysics Experiment for Physical Chemistry Students. J Chem Educ. 2010;87(9):961–964. https://doi.org/10.1021/ed900029c.
45. Ghisaidoobe AB, Chung SJ. Intrinsic Tryptophan Fluorescence in the Detection and Analysis of Proteins: A Focus on Förster Resonance Energy Transfer Techniques. Int J Mol Sci. 2014;15(12):22518–22538. https://doi.org/10.3390/ijms151222518.
46. Du X, Li Y, Xia Y-L, Ai S-M, Liang J, Sang P, Ji X-L, Liu S-Q. Insights into Protein–Ligand Interactions: Mechanisms, Models, and Methods. Int J Mol Sci. 2016;17(2):144. https://doi.org/10.3390/ijms17020144.
47. Platt EJ, Wehrly K, Kuhmann SE, Chesebro B, Kabat D. Effects of Ccr5 and Cd4 Cell Surface Concentrations on Infections by Macrophagetropic Isolates of Human Immunodeficiency Virus Type 1. J Virol. 1998;72(4):2855–2864. https://doi.org/10.1128/JVI.72.4.2855-2864.1998.
48. Sarzotti-Kelsoe M, Bailer RT, Turk E, Lin C, Bilska M, Greene KM, Gao H, Todd CA, Ozaki DA, Seaman MS, et al. Optimization and Validation of the Tzm-Bl Assay for Standardized Assessments of Neutralizing Antibodies against Hiv-1. J Immunol Methods. 2014;409:131–146. https://doi.org/10.1016/j.jim.2013.11.022.
49. Naidu D, Oduro-Kwateng E, Soliman MES, Ndlovu SI, Mkhwanazi NP. Alternaria Alternata (Fr) Keissl Crude Extract Inhibits Hiv Subtypes and Integrase Drug-Resistant Strains at Different Stages of Hiv Replication. Pharmaceuticals (Basel). 2025;18(2):189. https://doi.org/10.3390/ph18020189.
50. Kubheka MX, Ndlovu SI, Mkhwanazi NP. Anti-Hiv Activity and Immunomodulatory Properties of Fractionated Crude Extracts of Alternaria Alternata. Microorganisms. 2024;12(6):1150. https://doi.org/10.3390/microorganisms12061150.
51. Trott OV, Olson AJ. AutoDock Vina: improving the speed and accuracy of docking with a new scoring function, efficient optimization, and multithreading. J Comput Chem. 2010;31(2):455–461. https://doi.org/10.1002/jcc.21334.
52. Pettersen EF, Goddard TD, Huang CC, Couch GS, Greenblatt DM, Meng EC, Ferrin TE. Ucsf Chimera—a Visualization System for Exploratory Research and Analysis. J Comput Chem. 2004;25(13):1605–1612. https://doi.org/10.1002/jcc.20084.
53. Morris GM, Huey R, Lindstrom W, Sanner MF, Belew RK, Goodsell DS, Olson AJ. Autodock4 and Autodocktools4: Automated Docking with Selective Receptor Flexibility. J Comput Chem. 2009;30(16):2785–2791. https://doi.org/10.1002/jcc.21256.
54. Frisch MJ, Trucks GW, Schlegel HB, Scuseria GE, Robb MA, Cheeseman JR. Fox, D. J, *Gaussian 16, Revision C.01*. Wallingford (CT): Gaussian, Inc.; 2016.
55. Santos-Martins D, Solis-Vasquez L, Tillack AF, Sanner MF, Koch A, Forli S. Accelerating Autodock4 with Gpus and Gradient-Based Local Search. J Chem Theory Comput. 2021;17(2):1060–1073. https://doi.org/10.1021/acs.jctc.0c01006.
56. Nguyen NT, Nguyen TH, Pham TNH, Huy NT, Bay MV, Pham MQ, Nam PC, Vu VV, Ngo ST. Autodock Vina Adopts More Accurate Binding Poses but Autodock4 Forms Better Binding Affinity. J Chem Inf Model. 2020;60(1):204–211. https://doi.org/10.1021/acs.jcim.9b00778.
57. Motulsky H. Analyzing Data with Graphpad Prism. GraphPad Software Incorporated; 1999.
58. Cooper GM (editor). The Development and Causes of Cancer. In: The Cell: A Molecular Approach. 2nd Edition. Sunderland (MA): Sinauer Associates; 2000. https://www.ncbi.nlm.nih.gov/books/NBK9963/
59. Wang H, Wang F, Wang W, Yao X, Wei D, Cheng H, Deng Z. Improving the Expression of Recombinant Proteins in E. Coli Bl21 (De3) under Acetate Stress: An Alkaline Ph Shift Approach. PLoS One. 2014;9(11):e112777. https://doi.org/10.1371/journal.pone.0112777.
60. Bar-Magen T, Donahue DA, McDonough EI, Kuhl BD, Faltenbacher VH, Xu H, Michaud V, Sloan RD, Wainberg MA. Hiv-1 Subtype B and C Integrase Enzymes Exhibit Differential Patterns of Resistance to Integrase Inhibitors in Biochemical Assays. AIDS. 2010;24(14):2171–2179. https://doi.org/10.1097/QAD.0b013e32833cf265.
61. Jenkins TM, Engelman A, Ghirlando R, Craigie R. A Soluble Active Mutant of Hiv-1 Integrase: Involvement of Both the Core and Carboxyl-Terminal Domains in Multimerization. J Biol Chem. 1996;271(13):7712–7718. https://doi.org/10.1074/jbc.271.13.7712.

62. Hassounah SA, Liu Y, Quashie PK, Oliveira M, Moisi D, Brenner BG, Sandstrom PA, Mesplède T, Wainberg MA. Characterization of the Drug Resistance Profiles of Integrase Strand Transfer Inhibitors in Simian Immunodeficiency Virus Sivmac239. J Virol. 2015;89(23):12002–12013. https://doi.org/10.1128/JVI.02131-15.
63. Tramontano E, Colla PL, Cheng Y-C. Biochemical Characterization of the Hiv-1 Integrase 3 '-Processing Activity and Its Inhibition by Phosphorothioate Oligonucleotides. Biochemistry. 1998;37(20):7237–7243. https://doi.org/10.1021/bi972792o.
64. Malet I, Soulie C, Tchertanov L, Derache A, Amellal B, Traore O, Simon A, Katlama C, Mouscadet JF, Calvez V, et al. Structural Effects of Amino Acid Variations between B and Crf02-Ag Hiv-1 Integrases. J Med Virol. 2008;80(5):754–761. https://doi.org/10.1002/jmv.21169.
65. Lee SP, Kim HG, Censullo ML, Han MK. Characterization of Mg2+-Dependent 3'-Processing Activity for Human Immunodeficiency Virus Type 1 Integrase in Vitro: Real-Time Kinetic Studies Using Fluorescence Resonance Energy Transfer. Biochemistry. 1995;34(32):10205–10214. https://doi.org/10.1021/bi00032a014.
66. Métifiot M, Johnson BC, Kiselev E, Marler L, Zhao XZ, Burke TR Jr, Marchand C, Hughes SH, Pommier Y. Selectivity for Strand-Transfer over 3'-Processing and Susceptibility to Clinical Resistance of Hiv-1 Integrase Inhibitors Are Driven by Key Enzyme–DNA Interactions in the Active Site. Nucleic Acids Res. 2016;44(14):6896–6906. https://doi.org/10.1093/nar/gkw592.
67. Ebenhan T, Sathekge MM, Lengana T, Koole M, Gheysens O, Govender T, Zeevaart JR. 68ga-Nota-Functionalized Ubiquicidin: Cytotoxicity, Biodistribution, Radiation Dosimetry, and First-in-Human Pet/Ct Imaging of Infections. J Nucl Med. 2018;59(2):334–339. https://doi.org/10.2967/jnumed.117.200048.
68. Reddy N, Girdhari L, Shungube M, Gouws AC, Peters BK, Rajbongshi KK, Baijnath S, Mdanda S, Ntombela T, Arumugam T, et al. Neutralizing Carbapenem Resistance by Co-Administering Meropenem with Novel β-Lactam-Metallo-β-Lactamase Inhibitors. Antibiotics (Basel). 2023;12(4):633. https://doi.org/10.3390/antibiotics12040633.
69. Reddy N, Balieiro AM, Silva JRA, Gouws CA, Mutshembele A, Arvidsson PI, Kruger HG, Govender T, Naicker T. Navigating the Complexities of Drug Development for Metallo-β-Lactamase Inhibitors. RSC Med Chem. 2025;16(8):3393–3415. https://doi.org/10.1039/D5MD00035A.
70. Pham HT, Labrie L, Wijting IE, Hassounah S, Lok KY, Portna I, Goring ME, Han Y, Lungu C, van der Ende ME, et al. The S230r Integrase Substitution Associated with Virus Load Rebound during Dolutegravir Monotherapy Confers Low-Level Resistance to Integrase Strand-Transfer Inhibitors. J Infect Dis. 2018;218(5):698–706. https://doi.org/10.1093/infdis/jiy175.
71. Abdelhameed AS. Insight into the Interaction between the Hiv-1 Integrase Inhibitor Elvitegravir and Bovine Serum Albumin: A Spectroscopic Study. J Spectrosc. 2015;2015(1):435674. https://doi.org/10.1155/2015/435674.
72. Hutapea HML, Maladan Y, Widodo. Relationship between Hiv Integrase Polymorphisms and Integrase Inhibitor Susceptibility: An in Silico Analysis. Heliyon. 2018;4(12):e00956. https://doi.org/10.1016/j.heliyon.2018.e00956.
73. Isaacs D, Mikasi SG, Obasa AE, Ikomey GM, Shityakov S, Cloete R, Jacobs GB. Structural Comparison of Diverse Hiv-1 Subtypes Using Molecular Modelling and Docking Analyses of Integrase Inhibitors. Viruses. 2020;12(9):936. https://doi.org/10.3390/v12090936.
74. Sakkhachornphop S, Thongkum W, Tayapiwatana C. Novel 3'-Processing Integrase Activity Assay by Real-Time Pcr for Screening and Identification of Hiv-1 Integrase Inhibitors. BioMed Res Int. 2015;2015(1):853891. https://doi.org/10.1155/2015/853891.
75. Santos-Martins D, Forli S, Ramos MJ, Olson AJ. Autodock4zn: An Improved Autodock Force Field for Small-Molecule Docking to Zinc Metalloproteins. J Chem Inf Model. 2014;54(8):2371–2379. https://doi.org/10.1021/ci500209e.
76. Srinivasan B. A Guide to Enzyme Kinetics in Early Drug Discovery. FEBS J. 2023;290(9):2292–2305. https://doi.org/10.1111/febs.16404.